Theoretical Chemistry Accounts (2020) 139:161
https://doi.org/10.1007/s00214-020-02664-2

REGULAR ARTICLE

Computational mechanistic study on molecular catalysis of water oxidation by cyclam ligand-based iron complex

Koteswara Rao Gorantla[1] · **Bhabani S. Mallik**[1]

Received: 6 May 2020 / Accepted: 18 August 2020 / Published online: 20 September 2020

Abstract

The iron metal complexes containing cyclam-based macrocyclic ligands are active water oxidation catalysts, which can facilitate oxygen–oxygen bond formation during the water-splitting process. To understand the mechanism of the catalytic process, we explored this process by [Fe(cyclam)Cl_2]Cl performing density functional theory-based first-principles calculations. We examined the energetics of the formation of the oxygen–oxygen bond through the investigation of complexes $[Fe^{V}(cyclam)(O)_2]^{+,}$ and $[Fe^{V}(cyclam)(OH)(O)]^{+2}$. The process of water nucleophilic addition by this Fe^{V}–(oxo) complexes was explored in detail. Our computational study confirms the formation of these species, which were reported earlier in experimental conditions. The transition states for various reactions of the catalytic cycle were obtained within the implicit water model. From these calculations, we find that the proton transfers to cis–oxo or hydroxide moiety require high activation energy during the formation of the oxygen–oxygen bond. Our calculations reveal that the oxygen–oxygen bond formation by the transfer of a proton to the explicit water molecule requires more activation free energy than the transfer of a proton to the cis–oxo or hydroxide of the Fe^{V}–oxo species. Overall $[Fe^{V}(cyclam)(O)_2]^{+}$ and $[Fe^{V}(cyclam)(OH)(O)]^{+2}$ species with one explicit water molecule requires similar free energy. The Mulliken spin density data confirm the formation of the superoxide complexes. The activation free energy for the release of the oxygen molecule is lesser than that of the oxygen–oxygen bond formation. The natural bond orbital analysis for the complexes before and after the formation of the oxygen–oxygen bond formation shows that this bond formation happens through the interaction of antibonding orbital, $\pi^*(d^2_{x\ -y}{}^2\text{–}2p_y)$ of Fe=O moiety, with the σ*–orbital of the hydroxide group of the water molecule.

Keywords First-principles calculations · Water oxidation · Transition metal complex · Catalysis · Reaction mechanism

1 Introduction

The generation of fuels from the artificial photosynthesis process is one of the alternatives to fossil fuels to overcome major problems like the greenhouse effect [1, 2] and energy crisis [3]. In this process, the solar energy is accumulated in the form of chemical bonds by splitting the water molecule [4–7] into oxygen and hydrogen. The formed hydrogen can be used directly as a fuel or converted into another carbon-based fuel like methanol. In nature, the photosynthetic process converts carbon dioxide into carbohydrates through the use of solar energy and liberates oxygen. In Photosystem-II, P680 facilitates the transfer of electrons to the system, where carbon dioxide is reduced [8]. The oxidized P680 abstracted the four electrons from the Mn_4Ca cluster. After the transfer of four electrons, the Mn_4Ca cluster oxidizes the two moles of water into oxygen. The reaction proceeds through five oxidation states (S_0–S_4) by the creation of four oxidizing equivalents on the cluster during the water oxidation process. In this cycle, the S_0 state represents the most reduced, and the S_4 state is the most oxidized, and oxygen is released during the conversion of S_4 to S_0 state. [9] In contrast to natural photosynthesis, artificial photosynthetic catalysts oxidize water into chemical fuels like hydrogen. But, the formation of the oxygen–oxygen bond is a relatively high energetic barrier [7] process. An in-depth investigation of the mechanistic study of the complete catalytic cycle is

Electronic supplementary material The online version of this article (https://doi.org/10.1007/s00214-020-02664-2) contains supplementary material, which is available to authorized users.

✉ Bhabani S. Mallik
bhabani@chy.iith.ac.in

[1] Department of Chemistry, Indian Institute of Technology Hyderabad, Sangareddy, Telangana 502285, India

needed to understand this process. Molecular catalysts [10] have more advantages than metal oxides due to their ease of modification by chemical synthesis and able to incorporate into molecular assemblies for energy conversion systems. Bluedimmer (cis, cis-[$(bpy)_2(H_2O)Ru(\mu\text{-}O)\ Ru(H_2O)(bpy)_2]^{4-}$) [11, 12] is the first water oxidation catalyst (WOC) prepared by Meyer group. Later, many water oxidation catalysts of Ru [13–16] and Ir [17–21] were reported based on single and binuclear metal sites. The group of Tummel reported the single-site Ru [22]-based water oxidation catalyst with evidence of four-electron oxidation of water. Maji et al. [23] reported the single-site water catalyst based on Ru and explained about the effects of the hydrogen bond on the water oxidation process. These artificial molecular catalysts operate with a high turnover number (TON) under homogenous conditions [24], but limited abundance in the earth's crust and toxicity restrict them from being used on a large scale.

In order to make the water oxidation process viable, scientists developed earth-abundant first-row transition metals and especially iron-based WOCs. Collins and Bernhard [25] reported the iron-tetra amido macrocyclic ligand [TAMLs] complexes as the water oxidation catalysts; these complexes have a low turnover number (nearly 15), and Cramer group [26] studied the computational aspects of Fe-TAMLs. Fillol et al. [27] reported a large family of iron-based water oxidation systems and observed that those catalysts, which contain neutral tetradentate nitrogen-based ligands, and hydroxide group on the cis position was active toward water oxidation. Later, the same group studied the mechanism of WOCs computationally [28, 29]. Other iron-based catalysts were also reported for the purpose [30–32]. Nocera et al. [33] reported the cobalt hangman corrole complexes with meso-pentafluorophenyl substituents as the water oxidation catalyst. Rai Cao et al. [34, 35] reported the cobalt corroles as the catalysts for the oxygen evolution from the neutral aqueous solution. When phosphoric acid pendants substituted to these corroles, they facilitate both oxygen and hydrogen evolution reactions in the neutral aqueous solution. From the mechanistic study [36], it was observed that the carboxyl group in the second coordination sphere increased the catalytic activity of corroles. Not only iron [37, 38] and cobalt [33, 35, 39] but also other earth-abundant metals like manganese [24, 40–43] and nickel [44–46] containing complexes were also reported as the water oxidation catalysts.

Understanding the mechanistic nature of the existing catalyst through computationally is necessary for finding a better incentive for the water oxidation process. Primarily, the water oxidation process is carried by the addition of a water molecule as the nucleophile to the metal-oxo center in the single metal site complexes. DFT-based computational studies [30, 39, 47–51] can provide detailed catalytic cycle, redox potentials and nature of every oxidation state complementary to the experimental results. Many mechanistic questions like energies of intermediates and transition state structures can be answered through the quantum chemical calculations. Few studies were reported on the water oxidation process of the metal complex with explicit water molecules [36, 52–55]. Fillol et al. [28] studied the oxygen–oxygen bond formation with single and four explicit water molecules in two mechanistic pathways, and the results promote the internal base assistance of mechanism. The assessment of all the reactive processes involved in the water oxidation process requires a task that is difficult to accomplish to obtain a detailed understanding. Few of the goals were achieved by first-principles molecular metadynamics simulations [56], where we also studied the effect of the explicit water molecules on the mechanistic steps involved. This approach would require several trajectories and a high level of calculations leading to an expensive computational cost. The dynamical path can be evolved by identifying the stationary points from the minimum energy coordinate obtained from first-principles electronic structure calculations, which allow estimation of a variety of physicochemical parameters, comparable with experimental data.

In this study, we investigate the water oxidation process of the cyclam-based ligand with the iron metal center with single and four explicit water molecules within the M06L level of DFT, to compare with the results obtained from the more computationally demanding methods using the explicit water molecules. Some of these type ligands with the iron metal center were reported as the water oxidation catalysts in the presence of sacrificial oxidants like $NaIO_4$ or $NaClO_4$ at the moderate p^H value. Due to terminal hydrogen atoms, the catalysts are readily deactivated in the presence of cerium ammonium nitrate (pH 1) under harsh conditions of the water oxidation process. If the terminal hydrogen atoms of cyclam ligands are converted to methyl groups, the water oxidation capability increases tremendously. Tai-Chu Lau and co-workers studied the water oxidation of iron-based cross-bridged cyclam [57] ligand complexes. Kastrup et al. explored the water oxidation of these complexes as the electrocatalysts [58, 59]. Both studies reported that the water oxidation process occurs via Iron(V)–oxo species. Using UV/Vis data and ESI/MS results of bridged cyclam-Fe complexes in the water oxidation process, the authors found Fe(IV)-oxo species as the stable and dominated species, but these species are not involving in the water oxidation process. The Fe(V)=O species are readily involved in the water oxidation and dioxygen reduction process [60]. These high valance Fe complexes with other ligands are identified [61, 62] through the mass spectroscopy. To find the atomistic details of the mechanism and the involvement of Fe-bisoxo ($[Fe^V(cyclam)(O)_2]^+$) or Fe-oxo-hydroxide complex ($[Fe^V(cyclam)(O)\ (OH)]^{2+}$) in the water oxidation process, we performed DFT calculations considering

iron dichloro-1,4,8,11–tetraazacyclotetradecane (cis-[Fe (cyclam)Cl_2] Cl) [1] as the catalytic entity.

2 Computational methods

All the structures involved in the water oxidation catalytic process were optimized at the M06L [63] level using Gaussian09 [64] program. Double-zeta basis set SDD [65] was used for the iron and 6-31G(d,p) [66] for all other atoms. All the calculations were carried in an unrestricted manner and considered possible spin multiplicities for all the systems. The spin annihilation was rectified due to the spin contamination through quadratic convergence. The change in values of S^2 after the annihilation are around 1.5% as compared to earlier state. The effects of solvent were computed using the self-consistent reaction field method based on the polarizable conductor model. [67] We used water as a solvent (dielectric constant, $\varepsilon = 78.35$). When the reactions were carried out in the water medium, the solvent shows a more significant effect on reactivity. Truhlar and co-workers found a sufficient difference in Gibb's free energy calculations with and without optimization in the PCM model [68]. The saddle points in the gas and liquid phases are also different. Therefore, we carried both optimization and frequency calculations in the implicit solvent phase at an M06L electronic method level. The saddle points of all the structures were confirmed with no imaginary frequency, and transition states were identified with only one imaginary frequency. The single-point electronic energies were calculated with CC-pVTZ dunning basis set [69] for all atoms at the M06l level. The free energy corrections (G_{corr}) to the gas-phase calculations were taken from the frequency calculations at M06L/6-31G(d,p) (SDD for Fe) level on the optimized structure in the solvent phase (CPCM). All the free energies in solution were calculated as standard state of an ideal gas at a gas-phase concentration of 1 mol L^{-1} dissolving as an ideal dilute solution at a liquid phase concentration of 1 mol L^{-1}. For water, 55.6 M standard was employed [70]. For conversion of free energy from standard state gas–phase pressure of 1 atm to a standard state gas-phase concentration of 1 M, $\Delta G^{0/*}$ was added along with the previous corrections. The values of $\Delta G^{0/*}$ at 298 K are 1.9 and 4.3 kcal mol^{-1} for 1 M standard state solute and 55.6 M standard state water, respectively. The total Gibbs free energy was calculated as

$$G = E_{\text{cc-pVTZ}} + G_{\text{corr}} + \Delta G_{\text{Solv}} + \Delta G^{0/*}$$

The transition state was determined by using the Synchronous Transit-Guided Quasi-Newton method (QST2) [71] without guessing and confirmed by the IRC calculations. The change in free energy was calculated by taking the difference between the free energy of products and the reactants.

$$\left(\Delta G_{\text{sol}}\right)_{\text{reaction}} = \left(G_{\text{sol}}\right)_{\text{products}} - \left(G_{\text{sol}}\right)_{\text{reactants}}$$

The redox potential [72] was computed using a thermochemical cycle

$$\Delta G^{0}_{\text{sol}} = -E^{0}_{\text{sol}}\text{nF}$$

where F is the Faraday's constant and $\Delta G^{0}_{\text{sol}}$ is the free energy difference between reduced and oxidized species. In the present study, $\Delta G^{0}_{\text{sol}}$ was calculated by adding the solvation free energy difference ($\Delta\Delta G_{\text{sol}}$) to the free energy change in the gas phase, ΔG_{gas}. The obtained value was corrected with respect to standard hydrogen electrode potential (−4.24 eV). [73] Which is free energy change based on the Boltzmann statistics for the electron. The values of reduction potential are converted to experimental pH (=7) value by using the Nernst equation.

$$E = E^{0}_{\text{sol}} - \frac{RT}{F}\ln(10)\,X\,\frac{n_{H^+}}{n_e}\,X\,p^{H}$$

We computed the pK_a for an acid–base equilibrium in solution.

$$HA \rightarrow A^- + H^+$$

By using the thermochemical cycle [74] which was described earlier

$$\text{pKa} = \frac{\Delta G^{0}_{\text{deprot,(aq)}}}{RT\ln(10)}$$

where

$$\Delta G^{0}_{\text{deprot,aq}} = \left[\Delta G^{0}\left(A^{-}_{(\text{aq})}\right) - \Delta G^{0}_{\text{aq}}(HA) + \Delta G^{0}_{\text{aq}}\left(H^{+}\right)\right]$$

where $\Delta G^{0}_{\text{aq}} = \Delta G^{0}_{\text{g}} + \Delta G^{0}_{\text{sol}}$.

The free energy of solvation of a proton [73] taken as −265.9 kcal mol^{-1}, and a small gas-phase free energy correction of the proton taken as −6.3 kcal mol^{-1}

The transition state in the oxygen release was computed through the analysis of potential energy surface by the scanning of variation of energy with the change in iron-water and iron-dioxygen bonds. Natural bond orbital (NBO) [75] analysis was carried for $[Fe(cyclam)(O)_2]^+$ and $[Fe(cyclam)(O)(OH)]^{+2}$ in order to predict nature of the orbitals involved in the oxygen–oxygen bond formation by using NBO 3.0 [75] implemented in Gaussian program. All the energies reported are free energies until we mention separately. The spin multiplicities are shown on superscript of the particular catalytic intermediate.

3 Results and discussion

First, we explored the possibility of formation of $[Fe^{V}(cyclam)(O)_2]^{+}$ and $[Fe^{V}(cyclam)(O)(OH)]^{2+}$ complexes from the parent catalyst. Scheme 1 shows the conversion of $[Fe^{III}(cyclam)(H_2O)_2]^{3+}$to the Fe–oxo species. We evaluated the values of redox potentials and the pKa according to Scheme 1 at the pH 7. The formation of $[Fe^{IV}(cyclam)(H_2O)(O)]^{2+}$ through $[Fe^{III}(cyclam)(H_2O)_2]^{3+}$ by the two-proton-electron process requires the redox potential of 0.34 V. $[Fe^{IV}(cyclam)(O)(OH_2)]^{2+}$ is converted to $[Fe^{IV}(cyclam)(O)(OH)]^{+}$ with loss of a proton, with a pKa value of 4.2 log units. From $[Fe^{IV}(cyclam)(O)(OH)]^{+}$, $[Fe^{V}(cyclam)(O)_2]^{+}$ is formed through PCET with a computed potential of 1.02 V. $[Fe^{V}(cyclam)(O)(OH)]^{2+}$ is obtained from the $[Fe^{IV}(cyclam)(O)(H_2O)]^{2+}$ with a redox potential of 1.52 V, and the earlier reported Fe^{V}-bisoxo complex is formed from $[Fe^{V}(cyclam)(O)(OH)]^{+2}$ with a pKa value of 8.2 log units. The computed values of redox potentials correlate with the values obtained from experiments in the presence of sodium perchlorate or sodium periodate (considering 1.60 V vs. NHE). The computed values give evidence of the formation of Fe^{V}=O species. From the experimental observations, the evolution of oxygen was recorded at 1.8 V, which was higher than that of Fe^{+3}/Fe^{+4} (1.6 V vs. RHE). The results suggest that the +V oxidation state of Fe is required for the process. Some of the previous studies [60–62, 76] also suggested the formation of the Fe^{V}=O complexes, and the complexes were identified experimentally. Furthermore, we studied the nature of oxygen–oxygen bond formation through the $[Fe^{V}(cyclam)(O)(OH)]^{2+}$ and $[Fe^{V}(cyclam)(O)_2]^{+}$ species and the release of oxygen through a simple DFT-based thermodynamics for the catalytic cycles proposed in Schemes. In the catalytic cycle presented in Scheme 2a, the Fe^{V}–bisoxo complex (a_{oxo}) considered as the active catalytic species for the oxygen–oxygen bond formation. Scheme 2b represents the catalytic cycle with $[Fe^{V}(cyclam)(O)\ (OH)]^{2+}$($a_{OH}$) as an active catalytic species. For both catalytic cycles, we studied thermodynamics and kinetics of the oxygen–oxygen bond formation and release of the oxygen.

3.1 Mechanism of water oxidation

3.1.1 Oxygen–oxygen bond formation through $[Fe(cyclam)(O)_2]^{+}$ with a single explicit water molecule

The calculated values of redox potential and pKa of Scheme 1 confirm the formation of the catalytic active complex (a_{oxo}) $[Fe^{V}(cyclam)(O)_2]^{+}$. The formation of the oxygen–oxygen bond was studied in two possible ways. First, we considered a single explicit water molecule. The bond formed with assistance one of the oxo group of the a_{oxo} complex through a hydrogen bond. Secondly, we considered the transfer of hydrogen of a water molecule to another explicit water molecule. The quartet state of the a_{oxo} complex with one explicit water molecule is the ground state, which suggests that the iron with + 5 oxidation was stable with

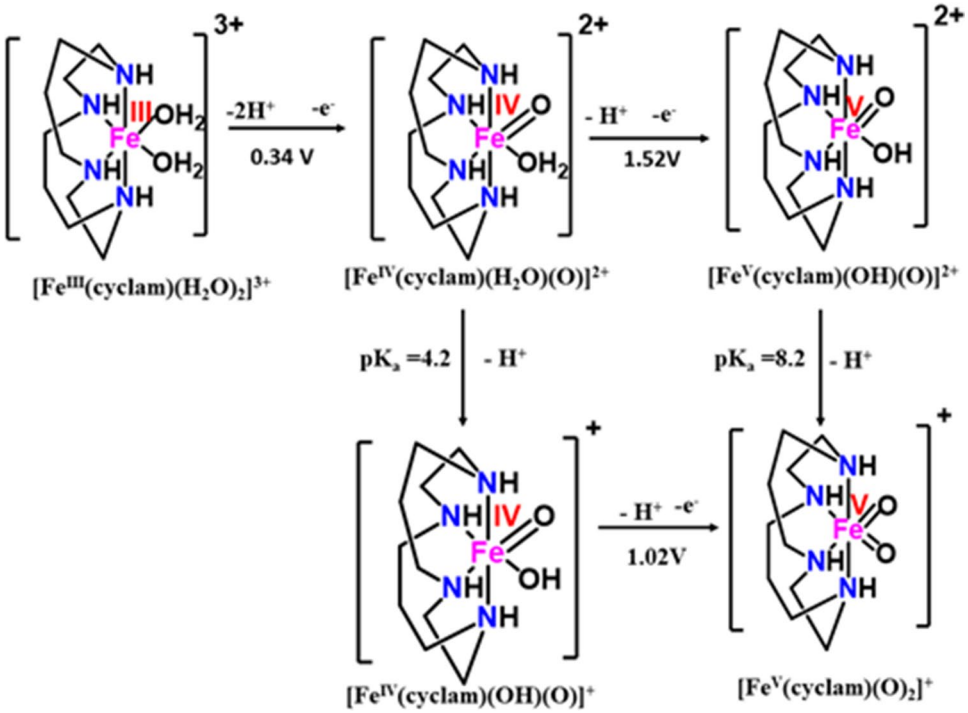

Scheme 1 The formation of high valent $[Fe^{V}(cyclam)(O)_2]^{+}$ and $[Fe^{V}(cyclam)(OH)(O)]^{2+}$ through proton-coupled electron transfer process

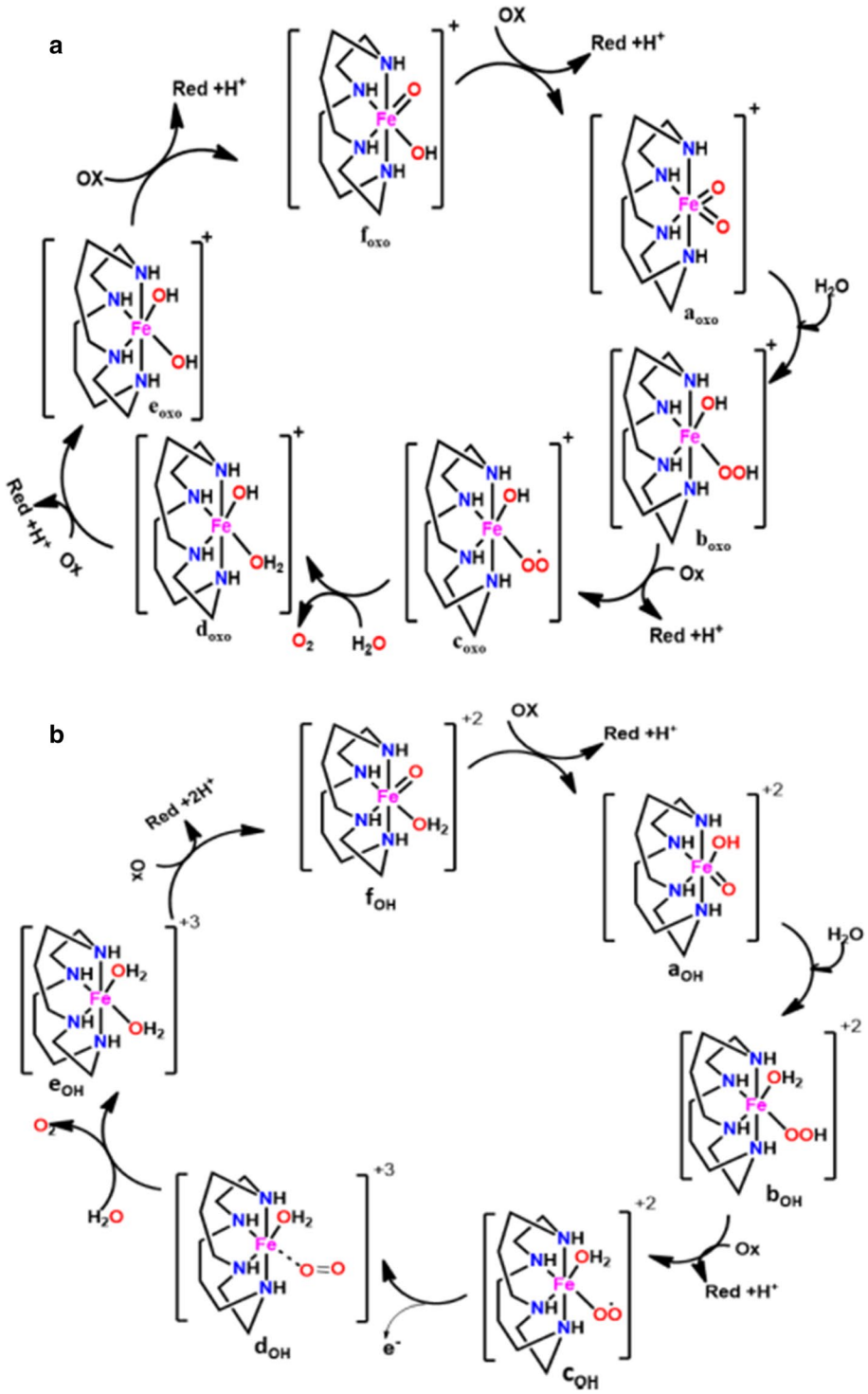

Scheme 2 **a** Catalytic cycle for oxygen–oxygen bond formation and release of oxygen through $[Fe^{V}(cyclam)(O)_2]^{+}$ (a_{oxo}) as the starting one, **b** catalytic cycle for oxygen–oxygen bond formation and release of oxygen through $[Fe^{V}(cyclam)(OH)(O)]^{+2}$ (a_{OH}) as the starting one

an electronic configuration of t_{2g}^{3} and e_{g}^{0}. Sextet and doublet states are the next higher energy spin states with 12.36 and 18.13 kcal mol^{-1}, respectively. Figure 1a shows the free energy profile for the oxygen–oxygen bond formation, along with structures of reactant, transition state and product. The two oxygen atoms of a_{oxo} complex form hydrogen bonds with the hydrogens atom, and the terminal hydrogen (of nitrogen) of the complex forms hydrogen bond with the oxygen atom of the water molecules. The length of both the iron-oxygen (Fe=O) bonds of a_{oxo} complex is 1.66 Å. The oxygen–oxygen bond results through a transition state (TS_{oxo}), which was computed through the QST2 method and confirmed by the IRC calculations. From the IRC curve (Fig. 1b), it is observed that one of the two hydrogen bonds

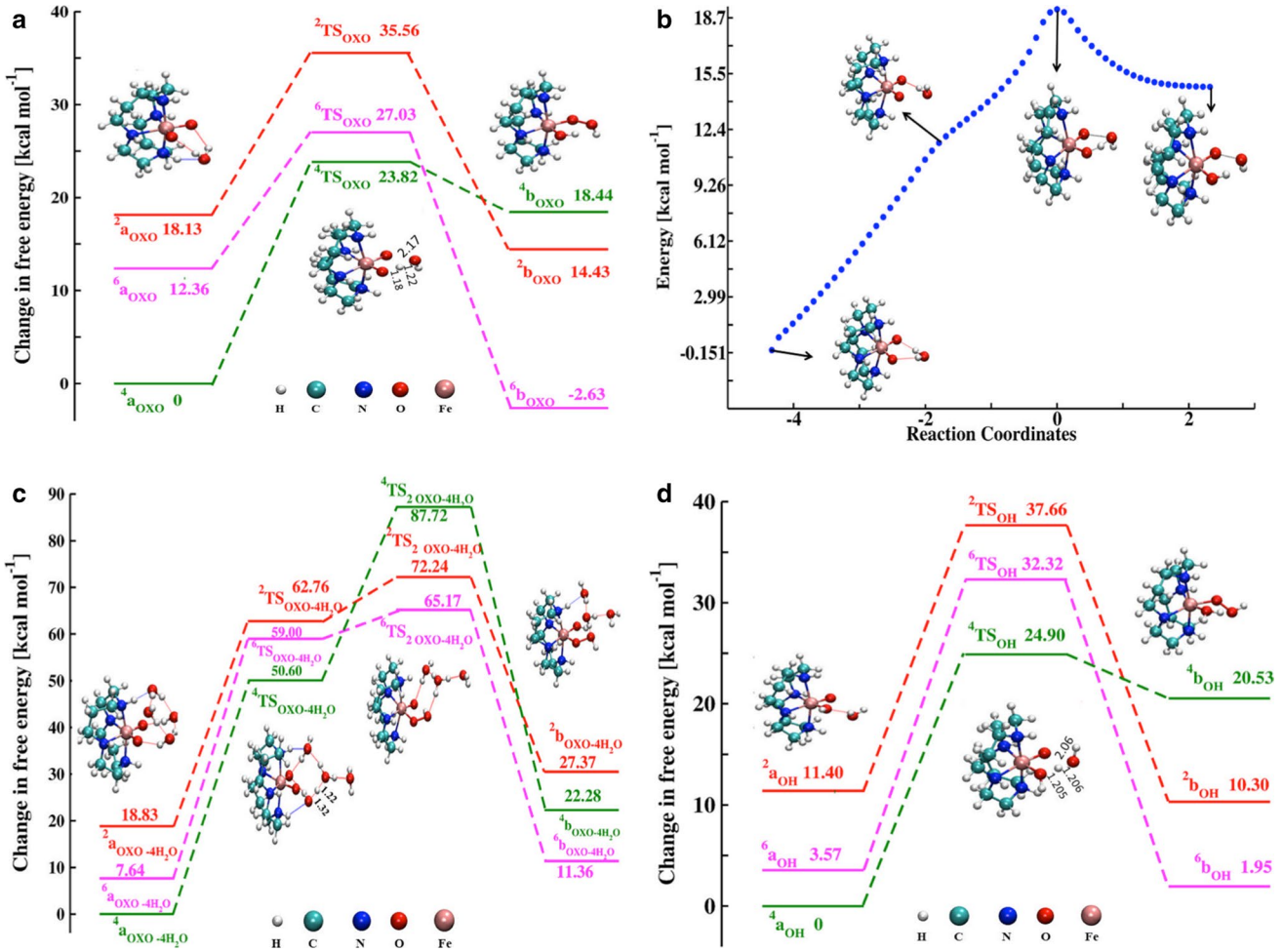

Fig. 1 **a** Free energy profile for oxygen–oxygen bond formation through $[Fe^{V}(cyclam)(O)_2]^{+}$ as the starting one, the free energies are reported relative to the quartet state of the complex $[Fe^{V}(cyclam)(O)_2]^{+}$. The multiplicity of each complex was shown on the superscript. **b** IRC path for oxygen–oxygen bond formation in the presence of a single explicit water molecule. Carried at M06L/SDD for Fe/6-31G(d,p) for other in CPCM (solvent model) $[Fe^{V}(cyclam)(O)_2]^{+}$ as the starting one with one explicit water molecule. **c** Free energy profile for oxygen–oxygen bond formation through $[Fe^{V}(cyclam)(O)_2]^{+}$ as the starting one in the presence of four explicit water molecule, the proton of one of the water molecule transfers to explicit water molecule. **d** Free energy profile for oxygen–oxygen bond formation through $[Fe^{V}(cyclam)(O)(OH)]^{2+}$ as the starting one, the free energies are reported relative to the quartet state of the complex $[Fe^{V}(cyclam)(O)(OH)]^{2+}$. The multiplicity of each complex is shown as the superscript

of the water with the two oxygen atoms is broken, and the corresponding water molecule orients itself to accommodate the change. The hydrogen-bonded hydrogen transfers to the oxo group of the a_{oxo} complex, and subsequently, the hydroxide migrates to the Fe=O moiety forming the oxygen–oxygen bond. Table 1 represents the spin densities of the atoms involved in the reaction, along with the bond lengths. The spin density of iron metal increases to 3.0662 from 1.9727 in the case of the transition state. The spin density on the oxygen atoms decreases to 0.2844 and −0.1536. The change in spin density values suggests that the addition of water molecule takes place as a nucleophile to the complex a_{oxo} forming $[Fe^{III}(cyclam)(OOH)(OH)]^{+}$ (b_{oxo}) complex. The spin density of iron decreases to 2.7653. From spin density values of oxygen atoms, it observed that the oxygen–oxygen bond is formed by the antiferromagnetic coupling of the oxo group with the hydroxide of the water molecule. The obtained complex, b_{oxo}, has sextet state as the ground state; quartet and doublet states are next higher energy spin states. The oxygen–oxygen bond length is 1.46 Å, and Fe–O oxygen bond length for iron peroxide is 1.84 Å. The activation free energy for the formation of oxygen–oxygen bond through the quartet state of the complex a_{oxo} is lower than the sextet and doublet state. The minimum activation energy value required for the formation of the thermodynamically favored bond is 23.82 kcal mol^{-1}, which is lesser than that of the previously reported value [26] based on the iron metal complexes.

Table 1 Mulliken spin densities of selected atoms and bond distances, in the formation of oxygen–oxygen bond through the $[Fe^{V}(cyclam)\ (O)_2]^{+}$ with quartet multiplicity

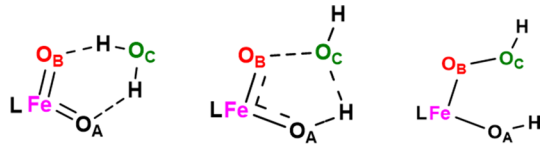

	Complex $^{4}a_{oxo}$	Transition states ($^{4}TS_{oxo}$)	Complex $^{4}b_{oxo}$
ρ (Fe)	1.9727	3.0662	2.7653
ρ (O_A)	0.5113	0.2844	0.0709
ρ (O_B)	0.5482	− 0.1536	0.4082
ρ (O_C)	0.0129	− 0.4347	− 0.0276
d (Fe–O_A) Å	1.66	1.73	1.84
d (Fe–O_B) Å	1.66	1.68	1.84
d (O_B–O_C) Å	2.84	2.17	1.46

3.1.2 Oxygen–oxygen bond formation through [Fe(cyclam) $(O)_2]^{+}$ with four explicit water molecule

In this section, we explore the mechanism of formation of the oxygen–oxygen bond by the transfer of a proton to one of the explicit water molecules. This type of mechanism requires at least four explicit water molecules to stabilize the formed hydronium ion through hydrogen-bonding. We considered four explicit water molecules present around the reaction center of the bisoxo complex $[[Fe(cyclam)(O)_2]^{+} + 4H_2O]$ (a_{OXO}-$4H_2O$). Figure 1c shows the free energy profile. The direct comparison of the energetics of different predicted spin states cannot be compared with any available experiments due to lack of relevant results; however, the involvement of intersystem crossing at the transition state that will allow the change of the spin state cannot be ruled out. The quartet state of the complex (a_{OXO}-$4H_2O$) is the ground state as compared to sextet and doublet states having next higher energy values of 7.64 and 18.83 kcal mol^{-1}, respectively. One of the water molecules close to the oxo group of the complex (a_{OXO}-$4H_2O$) facilitates the transfer of the proton to another explicit water molecule forming a transition state complex (TS_{OXO}-$4H_2O$). The ground state of this complex is the quartet spin state having the free energy of 50.60 kcal mol^{-1}. The transmitted proton to the water molecule forms the hydronium ion. The hydroxide is moved to the Fe–O moiety leading to the formation of the oxygen–oxygen bond in the transition state ($TS_{2\,OXO}$-$4H_2O$), and the spin density changes from 2.0145 to 3.0237 for iron. Table S1 of SI gives the spin density data; it informs that the electron density transfers to the Fe–O moiety. The Gibbs free energy barrier for the formation of TS_{2OXO}–$4H_2O$ is 65.17 kcal mol^{-1} for the sextet state. For the formation of the doublet and quartet states of the TS_{2OXO}–$4H_2O$ requires higher energy than the sextet state. The formed hydronium ion stabilizes by the hydrogen bond network formed by the other explicit water molecules and oxygen atoms of Fe–oxo-peroxide complex.

3.1.3 Oxygen–oxygen bond formation through [Fe(cyclam) $(O)(OH)]^{+2}$ with a single explicit water molecule

From the values of redox potentials and pKa of Scheme 1, the possibility of the formation of $[Fe^{V}(cyclam)(O)(OH)]^{+2}$ is confirmed. Spectroscopically evidence of Fe^{IV}-oxo species reported in some of the experimental studies [28, 57] based on water oxidation. These species can be converted to Fe^{V}-(O)(OH) by the proton-coupled electron transfer process. We studied the mechanism of formation of oxygen–oxygen bond in the presence of one single explicit water molecule with the assistance of cis–OH as an internal base. However, in the presence of four explicit water molecules, the hydrogen transfers to one of the water molecules instead of cis–OH. From the scheme 1, the formation of $[Fe^{V}(cyclam)(O)(OH)]^{+2}$ complex is possible under catalytic conditions. When this complex is optimized with one explicit water molecule, the hydrogen of the water molecule forms the hydrogen bond with the hydroxide group of the compound, which leads to a water adduct complex $[Fe^{V}(cyclam)\ (O)(OH)]^{+2}\ (H_2O)\ (a_{OH})$. Figure 1d shows a change in free energies relative to the $^{4}a_{OH}$, along with relative energies of the spin states. The quartet state of the complex is the ground state. Sextet and doublet states are the next higher energy states with 3.50 and 11.40 kcal mol^{-1} than the quartet state, respectively. The complex a_{OH} is converted to a hydroperoxide complex $[Fe^{III}(cyclam)(OOH)(OH_2)]^{+2}$ (b_{OH}) through the transition state with the formation of an oxygen–oxygen bond. The transition state for this conversion was computed through the QST2 method and confirmed by the IRC. By careful observation of the IRC curve (Figure S2 of SI), we find that first, the hydrogen atom of the water molecule is transferred to the cis–hydroxide moiety; later, the hydroxide migrates toward the oxygen atom of the Fe=O group. The formed transition state through the quartet state of complex a_{OH} is less energetic than the sextet and doublet states. Table S2 provides spin densities and varying bond lengths. The spin density of the iron metal center increases from 2.1340 to 2.8172; however, the Mulliken spin density on oxygen atom O_B is decreasing to 0.0723 (TS_{OH}) from 0.2092 (a_{OH}), which suggests the generation of the electrophilic nature at the oxygen atom O_B. Later the hydroxide of the water molecule is transferred to Fe-O_B moiety as a nucleophile and forms the oxygen–oxygen bond. The distance between O_B and O_C of the water in the transition state decreases to 2.06 from 3.05 Å, further decreases to 1.46 Å,

and forms the oxygen–oxygen bond. The spin density values of the oxygen atom, O_B, and O_C are shown in Table S2. The oxygen atoms are observed to be antiferromagnetically coupled with each other in the formation of the bond. The formed complex b_{OH} has a sextet state as the ground state, which has a free energy of 1.95 kcal mol^{-1} relative to $^4a_{OH}$. The quartet and doublet states of the b_{OH} are the next higher energy spin states with 20.53 and 10.30 kcal mol^{-1}, respectively. After the formation of the transition state, the spin crossover is observed. The activation free energy for the formation of the O–O bond, through the $^4a_{OH}$ complex via transition state ($^4TS_{OH}$), is the minimum barrier. The free energy barrier for this conversion is 24.90 kcal mol^{-1}. The free energy for this event through the sextet and doublet states of the complex a_{OH} requires higher energy than the quartet state. The formed transition state $^4TS_{OH}$ is the TOF determining transition state (TDTS) [77]. The free energy of the formation of oxygen–oxygen bond through cis–OH complex ($^4a_{OH}$) has nearly equal to the bisoxo ($^4a_{oxo}$) complex, which suggests that the oxygen–oxygen bond formation with a_{OH} is thermodynamically favorable.

3.1.4 Oxygen–oxygen bond formation through [Fe(cyclam)(O)(OH)]$^{+2}$ with four explicit water molecule

To explore the effects of solvents on the formation of the oxygen–oxygen bond, we considered four water molecules around the reaction center. In this mechanism, the transfer of hydrogen of a water molecule to another water molecule forms the hydronium ion. The explicit water molecules stabilize the formed hydronium ion with the hydrogen bond network. For this, we took four water molecules around the Fe-(O)(OH) moiety and optimized at M06L-level. Figure 2 displays a relative free energy profile for the formation of the oxygen–oxygen bond and proton transfer to another water molecule. The quartet state of the complex is the ground state of the complex ($[Fe^V(cyclam)(O)(OH)]^{+2} + 4H_2O$) ($4a_{OH}$-$4H_2O$). Sextet state and doublet states are the next higher energy states with 11.32 and 17.89 kcal mol^{-1}, respectively (Fig. 2). In this water adduct complex a_{OH}-$4H_2O$, the hydrogen of the hydroxide group makes the hydrogen bond with the oxygen of one of the water molecules. This hydrogen-bonded water molecule transfers the proton to another explicit water molecule through a transition state (TS_{OH}-$4H_2O$) with the free energy of 33.09 kcal mol^{-1} having quartet state as the ground state. The sextet and doublet states of the transition states are higher in free energy. From this stage, the proton transferred to another water molecule forms the hydronium ion, with concomitant of hydroxide transfer to the Fe=O moiety leads to the formation of an oxygen–oxygen bond. The resulted hydronium ion stabilizes by the hydrogen bond network of the other water molecules. The second transition state TS_{2OH}–$4H_2O$ has a sextet state as

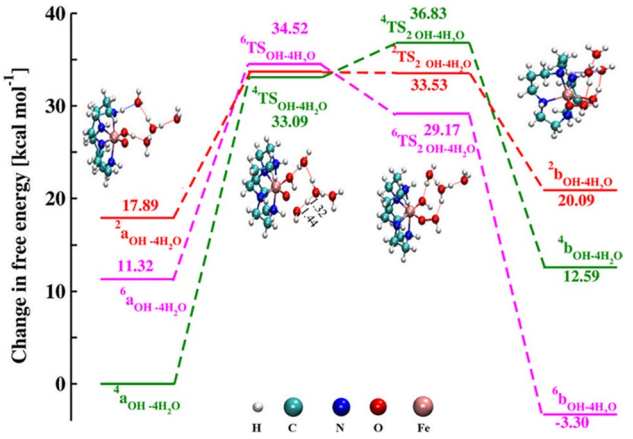

Fig. 2 Free energy profile for oxygen–oxygen bond formation through $[Fe^V(cyclam)(O)(OH)]^{+2}$ as the starting one in the presence of four explicit water molecule, the proton of one of the water molecule transfer to an explicit water molecule

the ground state. The oxygen–oxygen bond distance changes from 1.71 (TS_{OH}–$4H_2O$) to 1.47 Å (TS_{2OH} $4H_2O$) from the first transition state to the second one. The Mulliken spin density on the metal changes from 2.0653 to 2.9177 while changing from a quartet state of $^4a_{OH}$-$4H_2O$ to $^4TS_{OH}$–$4H_2O$. From $^4TS_{OH}$–$4H_2O$ to $^4TS_{2OH}$–$4H_2O$, the spin density varies very little. Table S3 of SI gives the spin densities and bond distances. By observing spin densities on the metal and oxygen atoms involved in the reaction, we see that the water is added to the Fe–O moiety as a nucleophile and noticed the spin crossover before the formation of the second transition state (TS_{2OH}–$4H_2O$). Finally, the proton from the hydronium ion is transferred to the cis–OH moiety through the Grotthuss mechanism [78] via hydrogen-bonded water molecule, which leads to the formation of the complex ($[Fe^{III}(cyclam)(OOH)(OH_2)]^{+2} + 3H_2O$) ($b_{OH}$-$4H_2O$). The formed complex ($b_{OH}$–$4H_2O$) has the sextet state as the ground state with -3.30 kcal mol^{-1} and the quartet, and doublet states are the next higher energy spin states with 12.59 and 20.09 kcal mol^{-1}, respectively, concerning $^4a_{OH}$-$4H_2O$. The TOF comparable rate-determining step is the formation of the transition state ($^4TS_{OH}$–$4H_2O$) with 33.09 kcal mol^{-1}, which is higher than the single explicit water molecule with $^4a_{OH}$. By comparing two mechanisms for the formation of the oxygen–oxygen bond by the $[Fe(cyclam)(O)(OH)]^{+2}$ species with the internal assistance of cis–OH is more favorable than the transfer of a proton to another specific water molecule.

By comparing the oxygen–oxygen bond formation through the a_{oxo} and a_{OH} complexes, internal base assistance with a single water molecule is more favorable. The internal base assistance by the cis–oxo is 1 kcal mol^{-1} less free energetic than the cis–OH case. The stability of the bisoxo complex in the experimental conditions may be

less, and the external base assistance through complex a_{OH} is more favorable. Complete molecular dynamic studies [56, 79] are required to get a clear understanding of the effect of explicit water molecules on the oxygen–oxygen bond formation. For that, we recently reported [56] the mechanistic study for the a_{oxo} and a_{OH} species. Due to the presence of the hydrogen bond cooperativity between the water molecules, the activation barrier decreases. But in both cases, the proton transfer to the cis–OH or oxo group is a less free energetic process than the transfer of the proton to another specific water molecule. This type of difference may be due to the level of the DFT and methodology adopted.

3.2 Molecular orbital diagram and natural bond orbital analysis

To understand which of the orbitals involved during the oxygen–oxygen bond of the water oxidation process, we performed the natural bond orbital (NBO) analysis for the complexes a_{OH} and the a_{oxo}. Figure 3 shows the orbitals for these complexes. In the molecular orbital diagram, we

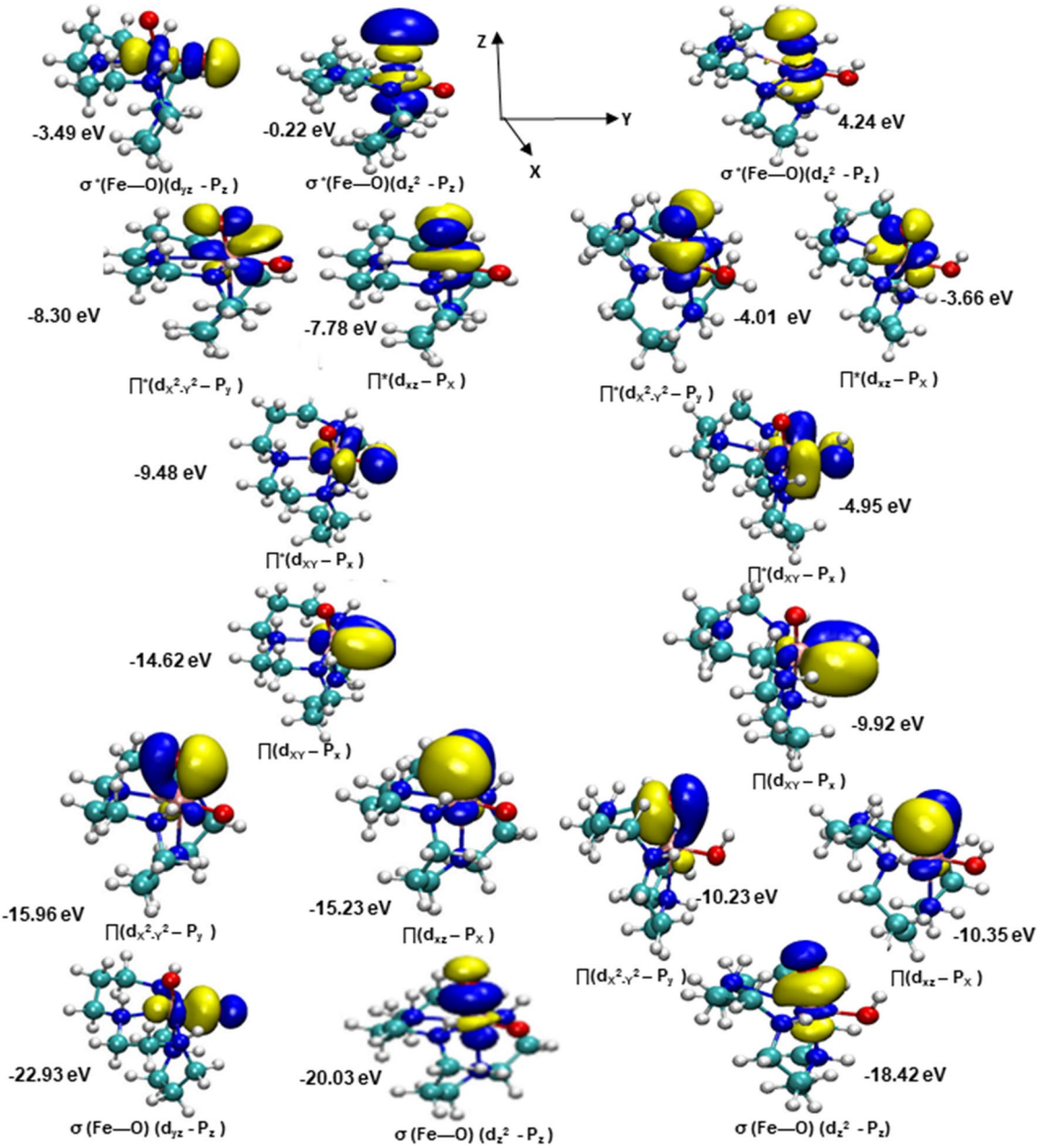

Fig. 3 Natural bond orbital analysis of $[Fe^{V}(cyclam)(O)_2]^{+}$ (left) and $[Fe^{V}(cyclam)(O)(OH)]^{+2}$ (right) orbitals are arranged in increasing order of their energies

mainly focus on the bonding nature of Fe=O bond. The d_z^2 and d_{yz} orbitals form sigma bonds with the oxygen atoms. The $d_{x^2-y^2}$ and d_{xz} orbitals form the π-bonding with the p_x and p_y orbitals of the oxygen atom. The d_{xy} orbital forms the π bonding with the $2p_x$ orbital of another oxygen atom of the complex a_{oxo}. The $d_{x^2-y^2}$ orbital of metal interacts with the $2p_y$ orbital of the oxygen atom. In the case of the complex a_{OH}, d_{xy} orbital forms π–antibonding with the $2p_x$ orbital of the oxygen atom of hydroxide moiety; this bond is due to the back bonding of oxygen p-orbital to d-orbital of metal. The d_{xz} orbital forms the π–antibonding with the $2p_x$ orbital of oxygen of the oxo group. The lowest unoccupied molecular orbital (LUMO) is $\pi^*(d_{x^2-y^2}-2p_y)$, which is one of π–antibonding orbital of the Fe=O moiety. These π*-orbitals are singly occupied, which can readily form the oxygen–oxygen bond. These orbitals overlap with the σ-orbital of the hydroxide of the water molecule to form the oxygen–oxygen σ-bond through the breaking one of the Fe–O π-bonds. In this bond formation, two-electron reduction in the metal center occurs with the addition of hydroxide as a nucleophile. From the natural charge analysis (NPA), we observe that the charge of the metal atom increases from 0.882 to 0.937, which suggests that the water added as a nucleophile to the Fe–O bond for the formation of the oxygen–oxygen bond. We further carried the NBO analysis of the complexes b_{oxo} and b_{OH} complexes; the study gives the evidence that the π^* ($d_{x^2-y^2} - 2p_y$) of Fe–O moiety is involved in oxygen–oxygen bond formation. The Fe–OOH bond forms by the interaction of $d_{x^2-y^2}$–orbital of the metal with the $2p_y$-orbital of the oxygen atom in the case of complex b_{oxo}. The analysis of the hybrid coefficients of the hybrid orbitals of natural atomic orbitals (NAO) of the Fe–O bond of peroxide (Fe-OOH moiety) of both complexes confirms that the oxygen–oxygen bond formation is due to the interaction of antibonding π^* ($d_{x^2-y^2} - 2p_y$) orbital with the σ^*–orbital of the water molecule. These are shown in supporting information Figure S3(SI).

3.3 Release of oxygen

The mechanistic pathway for the release of oxygen from the complexes b_{oxo} and b_{OH} was studied. From b_{oxo} complex, ($[Fe^{III}(cyclam)(OO.)(OH)]^{+1}$) ($c_{oxo}$) superoxide complex is formed through the PCET process with the potential of 0.46 V. The formed superoxide has the septet state as the ground state; the quintet and triplet states are next higher energy spin states. The spin density values on the oxygen atoms of the septet state are 0.6552 and 0.7471 on superoxide bond; moreover, the corresponding value on the oxygen of hydroxide is 0.3114. These values confirm the formation of superoxide (Fe^{III}–OO.) complex rather than a high valent peroxide bond. The formation of all three spin states of this complex is possible with perchlorate and periodate as the sacrificial oxidants. From complex b_{OH}, the superoxide complex also forms ($[Fe^{III}(cyclam)(OO^{\cdot})(OH_2)]^{+2}$) ($c_{OH}$) with the potential of 0.97 V. The c_{OH} complex has the ground state of septet state among other possible spin states. The spin densities of the septet sate of the c_{OH} complex are as follows: the metal center has 4.063, and the oxygen atoms of the superoxide oxygen atoms have 0.721 and 0.798. Figure 4 shows the spin density cubes. The conversion of the b_{oxo} into the tautomer c_{OH} has negative free energy, which can happen by the transfer of the hydrogen of Fe–OOH to the Fe–OH in the complex b_{oxo}. The c_{OH} is converted into ($[Fe^{III}(cyclam)(O=O)(OH_2)]^{+2}$) ($d_{OH}$), where forms the oxygen–oxygen double. This conversion requires the potential of 0.95 V. From this complex, the oxygen is released as dioxygen with an addition of water molecule and forms an intermediate catalytic complex ($[Fe^{III}(cyclam)(OH_2)(OH_2)]^{+3}$) ($e_{OH}$). The change in free energy for this step is 0.20 kcal mol^{-1}. The transition state for this conversion is identified through the potential energy scan (PES) method, by varying the bond lengths of iron-oxygen of dioxygen and oxygen of the incoming water molecule to iron metal center. The transition state is optimized at the same level as before, in both gas phase and implicit water phase (CPCM implicit water model), and confirmed with only one negative frequency. The activation free energy for this conversion is 4.02 kcal mol^{-1}. The release of the dioxygen molecule influenced by the explicit water molecules was studied by the Baerends et al. [54] for the Fe^{IV}=O complexes. Due to the Grotthus mechanism, the release of hydrogen peroxide is more dominant than the oxygen release. The authors studied the release of peroxide after the oxygen–oxygen bond formation without considering the formation of superoxide. In the current study, we discuss the case of the formation of superoxide, through which the release of the oxygen molecule happens. The spin density values suggest that the complexes C_{oxo} and C_{OH} complexes are in superoxide nature rather than the peroxide complexes, which can facilitate the release of dioxygen molecule than the peroxide. The formed e_{OH} is converted to ($[Fe^{IV}(cyclam)(O)(OH_2)]^{+2}$) ($f_{OH}$) through the PCET step with the reduction potential of 0.34 V.

The release of oxygen from the c_{oxo} complex by the addition of water molecule forms complex ($[Fe^{II}(cyclam)(OH)(OH_2)]^{+}$) ($d_{oxo}$) with free energy change of the 1.24 kcal mol^{-1}. The activation free energy for the release of dioxygen from the c_{oxo} complex by the addition of a water molecule is 6.60 kcal mol^{-1}. The formed d_{oxo} complex has a quintet state as the ground state, and triplet state is the next higher energy spin state. From the d_{oxo} complex, the bisoxo complex is regenerated through subsequent PCET steps. The complex d_{oxo} converts into bis-hydroxy ($[Fe^{III}(cyclam)(OH)(OH)]^{+}$)($e_{oxo}$) through the PCET process with a potential of 1.10 V. Later the e_{oxo} complex forms ($[Fe^{IV}(cyclam)(O)(OH)]^{+}$) ($f_{oxo}$) with a potential of 0.74 V. Finally, the bisoxo complex (a_{oxo}) is regenerated with the potential of 1.02 V

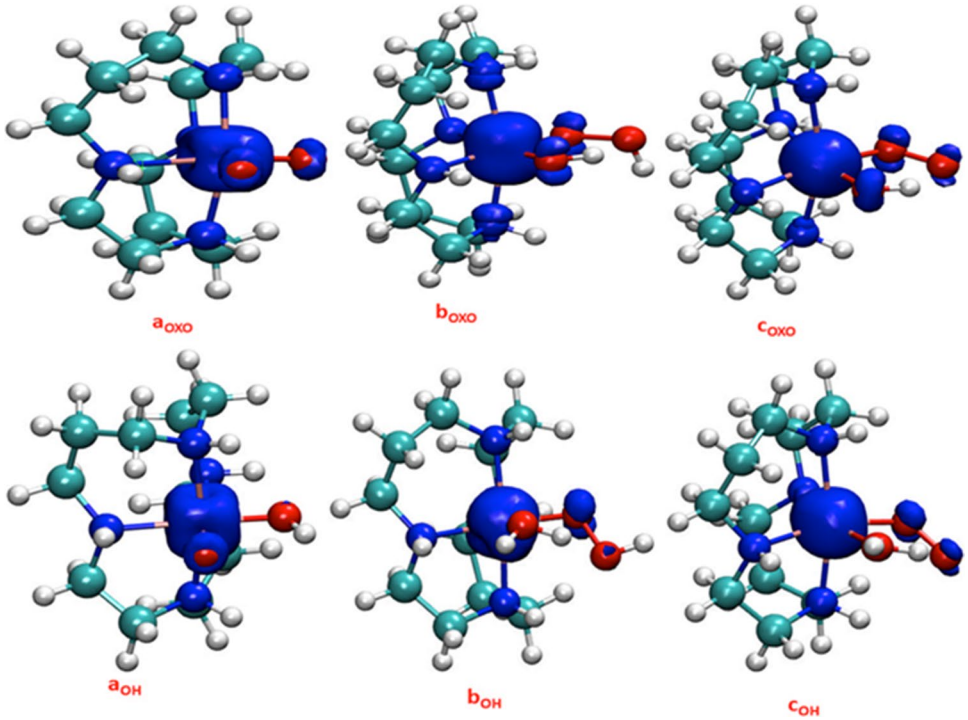

Fig. 4 Spin density plots for complexes $[Fe^{V}(cyclam)(O)_2]^{+}(a_{oxo})$, $[Fe^{III}(cyclam)(OH)(OOH)]^{+}$ (b_{oxo}) $[Fe^{III}(cyclam)(OH)(OO.)]^{+}(C_{oxo})$ $[Fe^{V}(cyclam)(O)(OH)]^{+2}(a_{OH})$, $[Fe^{III}(cyclam)(OOH)(OH_2)]^{+2}(b_{OH})$ $[Fe^{III}(cyclam)(OO.)(OH_2)]^{+2}$ (c_{OH}) all the cubes have the iso value-0.01

from f_{oxo}. The f_{oxo} intermediate can be formed through the comproportionation of the a_{oxo} and e_{oxo} compounds, with a negative free energy value. Like this, some of these reactions are expected to happen in the water at the experimental conditions.

$$\left[Fe^{III}(cyclam)(OOH)(OH)\right]^{+} + \left[Fe^{V}(cyclam)(O)_2\right]^{+} \rightarrow \left[Fe^{III}(cyclam)(OO^{\cdot})(OH)\right]^{+} + \left[Fe^{IV}(cyclam)(OH)(O)\right]^{+} \quad (1)$$

$$\left[Fe^{V}(cyclam)(O)(OH)\right]^{+2} + \left[Fe^{III}(cyclam)(OH)\left(OH_2\right)\right]^{+2} \rightarrow 2\left[Fe^{IV}(cyclam)(O)\left(OH_2\right)\right]^{+2} \quad (2)$$

$$Fe^{II}(cyclam)\left(OH_2\right)(OH)\right]^{+} + \left[Fe^{IV}(cyclam)(O)(OH)\right]^{+} \rightarrow 2\left[Fe^{III}(cyclam)(OH)(OH)\right]^{+} \quad (3)$$

$$Fe^{III}(cyclam)(OH)(OH)\right]^{+} + \left[Fe^{V}(cyclam)(O)_2\right]^{+} \rightarrow 2\left[Fe^{IV}(cyclam)(OH)(O)\right]^{+} \quad (4)$$

All these comproportionate reactions occur with negative free energy values. These types of reactions can be possible with the PCET [80] steps also. These reactions also give evidence of the formation of most of the catalytic intermediates. These types of reactions sometimes decrease the release of dioxygen due to the unavailability of higher oxidation states of metal complexes. Both catalytic cycles with four protons and four-electron transfer steps are shown in Figure S3 and Figure S4, along with the thermodynamic stages of oxygen–oxygen bond formation and release of oxygen. In both the catalytic process, the oxygen–oxygen bond formation is the rate-determining step. In the absence of availability of experimental value. The turn over frequency (TOF) [81] calculated from this energy span is 0.36 min^{-1}, which is comparable with earlier reported value [57] for similar complex.

4 Conclusions

We explore the water oxidation process of the cyclam-based iron metal that contains catalyst $[Fe^{III}(cyclam)(Cl)_2]Cl$, with the help of density functional theory at M06L-level. We focused mainly on the oxygen–oxygen bond formation through the $[Fe^{V}(cyclam)(O)(OH)]^{2+}$ and $[Fe^{V}(cyclam)(O)_2]^{2+}$ complexes. We examine the thermodynamics of this bond formation with one and four explicit water molecules separately. The bisoxo complex (a_{oxo}) with the quartet state

is the ground state. The minimum activation free energy for formation oxygen–oxygen bond required for a_{oxo} complex is found to be 23.82 kcal mol^{-1}; moreover, the required value was 24.90 kcal mol^{-1} in the case of $[Fe^{V}(cyclam)(O)(OH)]^{2+}$. From the NBO analysis of the complexes a_{oxo} and a_{OH}, it is observed that the antibonding orbital ($\pi^*(d^2_{x-y^2}-2p_y)$) of Fe–O moiety interacting with the σ*-orbital of the hydroxide group leads to the formation of peroxide complex. We examine the water oxidation process of these complexes by transfer of a proton to the explicit water molecule, hydroxide, to the Fe-oxo moiety. The mechanism involving four water molecules requires higher free energy than earlier, which can be thermodynamically unviable. Overall the oxygen–oxygen bond formation through one explicit water molecule with bisoxo complex was more favorable. The peroxide complex was converted into a superoxide complex through the proton-coupled electron transfer reaction. We also investigate the Mulliken spin density analysis of the superoxide nature of the O–O bond. Later, we examine the release of the dioxygen. The energetics of the release of oxygen from the complex d_{OH} is lesser than the c_{oxo} complex, but the interconversion between the b_{oxo} to the c_{OH} was a free energetic process. Finally, the release of dioxygen requires minimum activation energy of 4.02 kcal mol^{-1}. From thermodynamic data, the overall rate-determining step is the oxygen–oxygen bond formation for both the catalytic cycles. While comparing with our previous [56] results based on the water oxidation process in the presence of the explicit water molecules, the rate demining step is the oxygen–oxygen bond formation in both the cases. The activation free energy decreases in the presence of explicit water for both the conditions. However, the effect was less for other steps. Mainly the thermodynamic steps are more influenced by the explicit water than the kinetic steps like PCET. This is due to the cooperativity of the water molecules through the hydrogen bonds. Our mechanistic study may provide mechanistic insight and help in the development of water oxidation catalysts based on cyclam-based ligands.

Acknowledgements This research was supported by the Indian Institute of Technology Hyderabad (IITH). G. Koteswara Rao likes to thank UGC, India, for his Ph.D. fellowship.

Compliance with ethical standards

Conflict of interest The authors declare no competing financial interest.

References

1. Riffat SBMA (2015) Building energy consumption and carbon dioxide emissions: threat to climate change. J Earth Sci Clim Change. https://doi.org/10.4172/2157-7617.S3-001
2. Tollefson J (2011) How green is my future? Nature 473:134–135. https://doi.org/10.1038/473134a
3. Cook TR, Dogutan DK, Reece SY et al (2010) Solar energy supply and storage for the legacy and nonlegacy worlds. Chem Rev 110:6474–6502. https://doi.org/10.1021/cr100246c
4. Liu J, Liu Y, Liu N et al (2015) Metal-free efficient photocatalyst for stable visible water splitting via a two-electron pathway. Science 347:970–974. https://doi.org/10.1126/science.aaa3145
5. Balzani V, Credi A, Venturi M (2008) Photochemical conversion of solar energy. ChemSusChem 1:26–58. https://doi.org/10.1002/cssc.200700087
6. Barber J (2009) Photosynthetic energy conversion: natural and artificial. Chem Soc Rev 38:185–196. https://doi.org/10.1039/b802262n
7. Gust D, Moore TA, Moore AL (2009) Solar fuels via artificial photosynthesis. Acc Chem Res 42:1890–1898. https://doi.org/10.1021/ar900209b
8. Dismukes GC, Brimblecombe R, Felton GAN et al (2009) Development of bioinspired Mn4O4− Cubane water oxidation catalysts: lessons from photosynthesis. Acc Chem Res 42:1935–1943. https://doi.org/10.1021/ar900249x
9. Kok B, Forbush B, McGloin M (1970) Cooperation of charges in photosynthetic O_2 evolution-I. A linear four step mechanism. Photochem Photobiol 11:457–475. https://doi.org/10.1111/j.1751-1097.1970.tb06017.x
10. Blakemore JD, Crabtree RH, Brudvig GW (2015) Molecular catalysts for water oxidation. Chem Rev 115:12974–13005. https://doi.org/10.1021/acs.chemrev.5b00122
11. Liu F, Concepcion JJ, Jurss JW et al (2008) Mechanisms of water oxidation from the blue dimer to photosystem II. Inorg Chem 47:1727–1752. https://doi.org/10.1021/ic701249s
12. Gersten SW, Samuels GJ, Meyer TJ (1982) Catalytic oxidation of water by an oxo-bridged ruthenium dimer. J Am Chem Soc 104:4029–4030. https://doi.org/10.1021/ja00378a053
13. Concepcion JJ, Jurss JW, Templeton JL, Meyer TJ (2008) One site is enough. Catalytic water oxidation by $[Ru(tpy)(bpm)(OH2)]^{2+}$ and $[Ru(tpy)(bpz)(OH2)]^{2+}$. J Am Chem Soc 130:16462–16463. https://doi.org/10.1021/ja8059649
14. Neudeck S, Maji S, López I et al (2016) Establishing the family of diruthenium water oxidation catalysts based on the bis(bipyridyl)pyrazolate ligand system. Inorg Chem 55:2508–2521. https://doi.org/10.1021/acs.inorgchem.5b02869
15. Masaoka S, Sakai K (2009) Clear evidence showing the robustness of a highly active oxygen-evolving mononuclear ruthenium complex with an aqua ligand. Chem Lett 38:182–183. https://doi.org/10.1246/cl.2009.182
16. Hirahara M, Ertem MZ, Komi M et al (2013) Mechanisms of photoisomerization and water-oxidation catalysis of mononuclear ruthenium(II) monoaquo complexes. Inorg Chem 52:6354–6364. https://doi.org/10.1021/ic400054k
17. Blakemore JD, Schley ND, Balcells D et al (2010) Half-sandwich iridium complexes for homogeneous water-oxidation catalysis. J Am Chem Soc 132:16017–16029. https://doi.org/10.1021/ja104775j
18. DePasquale J, Nieto I, Reuther LE et al (2013) Iridium dihydroxybipyridine complexes show that ligand deprotonation dramatically speeds rates of catalytic water oxidation. Inorg Chem 52:9175–9183. https://doi.org/10.1021/ic302448d
19. Hull JF, Balcells D, Blakemore JD et al (2009) Highly active and robust Cp* Iridium complexes for catalytic water oxidation. J Am Chem Soc 131:8730–8731. https://doi.org/10.1021/ja901270f
20. Lalrempuia R, McDaniel ND, Müller-Bunz H et al (2010) Water oxidation catalyzed by strong carbene-type donor-ligand complexes of iridium. Angew Chem Int Ed 49:9765–9768. https://doi.org/10.1002/anie.201005260
21. McDaniel ND, Coughlin FJ, Tinker LL, Bernhard S (2008) Cyclometalated iridium(III) aquo complexes: efficient and

tunable catalysts for the homogeneous oxidation of water. J Am Chem Soc 130:210–217. https://doi.org/10.1021/ja074478f
22. López I, Ertem MZ, Maji S et al (2014) A self-improved water-oxidation catalyst: is one site really enough? Angew Chem Int Ed 53:205–209. https://doi.org/10.1002/anie.201307509
23. Maji S, López I, Bozoglian F et al (2013) Mononuclear ruthenium–water oxidation catalysts: discerning between electronic and hydrogen-bonding effects. Inorg Chem 52:3591–3593. https://doi.org/10.1021/ic3028176
24. Kärkäs MD, Åkermark B (2016) Water oxidation using earth-abundant transition metal catalysts: opportunities and challenges. Dalton Trans 45:14421–14461. https://doi.org/10.1039/C6DT00809G
25. Ellis WC, McDaniel ND, Bernhard S, Collins TJ (2010) Fast water oxidation using iron. J Am Chem Soc 132:10990–10991. https://doi.org/10.1021/ja104766z
26. Ertem MZ, Gagliardi L, Cramer CJ (2012) Quantum chemical characterization of the mechanism of an iron-based water oxidation catalyst. Chem Sci 3:1293–1299. https://doi.org/10.1039/C2SC01030E
27. Fillol JL, Codolà Z, Garcia-Bosch I et al (2011) Efficient water oxidation catalysts based on readily available iron coordination complexes. Nat Chem 3:807–813. https://doi.org/10.1038/nchem.1140
28. Acuña-Parés F, Costas M, Luis JM, Lloret-Fillol J (2014) Theoretical study of the water oxidation mechanism with non-heme Fe(Pytacn) iron complexes. Evidence that the FeIV(O)(Pytacn) species cannot react with the water molecule to form the O–O bond. Inorg Chem 53:5474–5485. https://doi.org/10.1021/ic500108g
29. Acuña-Parés F, Codolà Z, Costas M et al (2014) Unraveling the mechanism of water oxidation catalyzed by nonheme iron complexes. Chem Eur J 20:5696–5707. https://doi.org/10.1002/chem.201304367
30. Annunziata A, Esposito R, Gatto G et al (2018) Iron(III) complexes with cross-bridged cyclams: synthesis and use in alcohol and water oxidation catalysis. Eur J Inorg Chem 2018:3304–3311. https://doi.org/10.1002/ejic.201800451
31. Kottrup KG, D'Agostini S, van Langevelde PH et al (2018) Catalytic activity of an iron-based water oxidation catalyst: substrate effects of graphitic electrodes. ACS Catal 8:1052–1061. https://doi.org/10.1021/acscatal.7b03284
32. Sinha W, Mahammed A, Fridman N, Gross Z (2020) Water oxidation catalysis by mono- and binuclear iron corroles. ACS Catal 10:3764–3772. https://doi.org/10.1021/acscatal.9b05382
33. McGuire R Jr, Dogutan DK, Teets TS et al (2010) Oxygen reduction reactivity of cobalt(II) hangman porphyrins. Chem Sci 1:411–414. https://doi.org/10.1039/C0SC00281J
34. Sinha W, Mizrahi A, Mahammed A et al (2018) Reactive intermediates involved in cobalt corrole catalyzed water oxidation (and oxygen reduction). Inorg Chem 57:478–485. https://doi.org/10.1021/acs.inorgchem.7b02696
35. Sun H, Han Y, Lei H et al (2017) Cobalt corroles with phosphonic acid pendants as catalysts for oxygen and hydrogen evolution from neutral aqueous solution. Chem Commun 53:6195–6198. https://doi.org/10.1039/C7CC02400B
36. Ertem MZ, Cramer CJ (2012) Quantum chemical characterization of the mechanism of a supported cobalt-based water oxidation catalyst. Dalton Trans 41:12213–12219. https://doi.org/10.1039/C2DT31871G
37. Chen G, Chen L, Ng S-M et al (2013) Chemical and visible-light-driven water oxidation by iron complexes at pH 7–9: evidence for dual-active intermediates in iron-catalyzed water oxidation. Angew Chem Int Ed 52:1789–1791. https://doi.org/10.1002/anie.201209116
38. Hoffert WA, Mock MT, Appel AM, Yang JY (2013) Incorporation of hydrogen-bonding functionalities into the second coordination sphere of iron-based water-oxidation catalysts. Eur J Inorg Chem 2013:3846–3857. https://doi.org/10.1002/ejic.201201499
39. Schilling M, Luber S (2018) Computational modeling of cobalt-based water oxidation: current status and future challenges. Front Chem 6:1–21. https://doi.org/10.3389/fchem.2018.00100
40. Sala X, Maji S, Bofill R et al (2014) Molecular water oxidation mechanisms followed by transition metals: state of the art. Acc Chem Res 47:504–516. https://doi.org/10.1021/ar400169p
41. Zhang C, Chen C, Dong H et al (2015) A synthetic Mn4Ca-cluster mimicking the oxygen-evolving center of photosynthesis. Science 348:690–693. https://doi.org/10.1126/science.aaa6550
42. Fernando A, Aikens CM (2016) Theoretical investigation of water oxidation catalysis by a model manganese cubane complex. J Phys Chem C 120:21148–21161. https://doi.org/10.1021/acs.jpcc.6b03029
43. Chen C, Li Y, Zhao G et al (2017) Natural and artificial Mn4Ca cluster for the water splitting reaction. ChemSusChem 10:4403–4408. https://doi.org/10.1002/cssc.201701371
44. Lin J, Kang P, Liang X et al (2017) Homogeneous electrocatalytic water oxidation catalyzed by a mononuclear nickel complex. Electrochim Acta 258:353–359. https://doi.org/10.1016/j.electacta.2017.11.061
45. Wang L, Duan L, Ambre RB et al (2016) A nickel (II) PY5 complex as an electrocatalyst for water oxidation. J Catal 335:72–78. https://doi.org/10.1016/j.jcat.2015.12.003
46. Wang D, Bruner CO (2017) Catalytic water oxidation by a bio-inspired nickel complex with a redox-active ligand. Inorg Chem 56:13638–13641. https://doi.org/10.1021/acs.inorgchem.7b02166
47. Cramer CJ, Truhlar DG (2009) Density functional theory for transition metals and transition metal chemistry. Phys Chem Chem Phys 11:10757–10816. https://doi.org/10.1039/B907148B
48. Sameera WMC, Maseras F (2012) Transition metal catalysis by density functional theory and density functional theory/molecular mechanics. WIREs Comput Mol Sci 2:375–385. https://doi.org/10.1002/wcms.1092
49. Thiel W (2014) Computational catalysis—past, present, and future. Angew Chem Int Ed 53:8605–8613. https://doi.org/10.1002/anie.201402118
50. Pidko EA (2017) Toward the balance between the reductionist and systems approaches in computational catalysis: model versus method accuracy for the description of catalytic systems. ACS Catal 7:4230–4234. https://doi.org/10.1021/acscatal.7b00290
51. Esposito R, Raucci U, Cucciolito ME et al (2019) Iron(III) complexes for highly efficient and sustainable ketalization of glycerol: a combined experimental and theoretical study. ACS Omega 4:688–698. https://doi.org/10.1021/acsomega.8b02546
52. Ma C, Piccinin S, Fabris S (2012) Reaction mechanisms of water splitting and H2 evolution by a Ru(II)-pincer complex identified with ab initio metadynamics simulations. ACS Catal 2:1500–1506. https://doi.org/10.1021/cs300350b
53. Raucci U, Ciofini I, Adamo C, Rega N (2016) Unveiling the reactivity of a synthetic mimic of the oxygen evolving complex. J Phys Chem Lett 7:5015–5021. https://doi.org/10.1021/acs.jpclett.6b02144
54. Bernasconi L, Kazaryan A, Belanzoni P, Baerends EJ (2017) Catalytic oxidation of water with high-spin iron(IV)–oxo species: role of the water solvent. ACS Catal 7:4018–4025. https://doi.org/10.1021/acscatal.7b00568
55. Liao R-Z, Siegbahn PEM (2017) Possible water association and oxidation mechanisms for a recently synthesized Mn4Ca-complex. J Catal 354:169–181. https://doi.org/10.1016/j.jcat.2017.07.016
56. Gorantla KR, Mallik BS (2020) Iron complex as a water-oxidizing catalyst: free-energy barriers, proton-coupled electron transfer, spin dynamics, and role of water molecules in the reaction

mechanism. J Phys Chem C 124:205–218. https://doi.org/10.1021/acs.jpcc.9b10378
57. Tan P, Kwong H-K, Lau T-C (2015) Catalytic oxidation of water and alcohols by a robust iron(III) complex bearing a cross-bridged cyclam ligand. Chem Commun 51:12189–12192. https://doi.org/10.1039/C5CC02868J
58. Hetterscheid DGH (2017) In operando studies on the electrochemical oxidation of water mediated by molecular catalysts. Chem Commun 53:10622–10631. https://doi.org/10.1039/C7CC04944G
59. Kottrup KG, Hetterscheid DGH (2016) Evaluation of iron-based electrocatalysts for water oxidation—an on-line mass spectrometry approach. Chem Commun 52:2643–2646. https://doi.org/10.1039/C5CC10092E
60. Ray K, Heims F, Schwalbe M, Nam W (2015) High-valent metal-oxo intermediates in energy demanding processes: from dioxygen reduction to water splitting. Curr Opin Chem Biol 25:159–171. https://doi.org/10.1016/j.cbpa.2015.01.014
61. dos Santos MR, Diniz JR, Arouca AM et al (2012) Ionically tagged iron complex-catalyzed epoxidation of olefins in imidazolium-based ionic liquids. ChemSusChem 5:716–726. https://doi.org/10.1002/cssc.201100453
62. dos Santos MR, Gomes AF, Gozzo FC et al (2012) Iron complex with ionic tag-catalyzed olefin reduction under oxidative conditions—a different reaction for iron. ChemSusChem 5:2383–2389. https://doi.org/10.1002/cssc.201200344
63. Zhao Y, Truhlar DG (2006) A new local density functional for main-group thermochemistry, transition metal bonding, thermochemical kinetics, and noncovalent interactions. J Chem Phys 125:194101. https://doi.org/10.1063/1.2370993
64. Frisch MJ, Trucks GW, Schlegel HB, Scuseria GE, Robb MA, Cheeseman JR, Scalmani G, Barone V, Mennucci B, Petersson GA, Nakatsuji H, Caricato M, Li X, Hratchian HP et al. Gaussian 09, revision C.01
65. Dolg M, Wedig U, Stoll H, Preuss H (1987) Energy-adjusted ab initio pseudopotentials for the first row transition elements. J Chem Phys 86:866–872. https://doi.org/10.1063/1.452288
66. Rassolov VA, Pople JA, Ratner MA, Windus TL (1998) 6-31G* basis set for atoms K through Zn. J Chem Phys 109:1223–1229. https://doi.org/10.1063/1.476673
67. Barone V, Cossi M (1998) Quantum calculation of molecular energies and energy gradients in solution by a conductor solvent model. J Phys Chem A 102:1995–2001. https://doi.org/10.1021/jp9716997
68. Ribeiro RF, Marenich AV, Cramer CJ, Truhlar DG (2011) Use of solution-phase vibrational frequencies in continuum models for the free energy of solvation. J Phys Chem B 115:14556–14562. https://doi.org/10.1021/jp205508z
69. Weigend F, Ahlrichs R (2005) Balanced basis sets of split valence, triple zeta valence and quadruple zeta valence quality for H to Rn: design and assessment of accuracy. Phys Chem Chem Phys 7:3297–3305. https://doi.org/10.1039/B508541A
70. Kelly CP, Cramer CJ, Truhlar DG (2006) Adding explicit solvent molecules to continuum solvent calculations for the calculation of aqueous acid dissociation constants. J Phys Chem A 110:2493–2499. https://doi.org/10.1021/jp055336f
71. Peng C, Schlegel HB (1993) Combining synchronous transit and quasi-newton methods to find transition states. Isr J Chem 33:449–454. https://doi.org/10.1002/ijch.199300051
72. Baik M-H, Friesner RA (2002) Computing redox potentials in solution: density functional theory as a tool for rational design of redox agents. J Phys Chem A 106:7407–7412. https://doi.org/10.1021/jp025853n
73. Kelly CP, Cramer CJ, Truhlar DG (2007) Single-ion solvation free energies and the normal hydrogen electrode potential in methanol, acetonitrile, and dimethyl sulfoxide. J Phys Chem B 111:408–422. https://doi.org/10.1021/jp0654031
74. Jang YH, Goddard WA, Noyes KT et al (2003) pKa values of guanine in water: density functional theory calculations combined with Poisson–Boltzmann continuum–solvation model. J Phys Chem B 107:344–357. https://doi.org/10.1021/jp020774x
75. Glendening ED, Reed AE, Carpenter JE, Weinhold F (1998) NBO version 3.1, TCI. University of Wisconsin, Madison
76. Hohenberger J, Ray K, Meyer K (2012) The biology and chemistry of high-valent iron–oxo and iron–nitrido complexes. Nat Commun 3:720. https://doi.org/10.1038/ncomms1718
77. Kozuch S, Shaik S (2011) How to conceptualize catalytic cycles? The energetic span model. Acc Chem Res 44:101–110. https://doi.org/10.1021/ar1000956
78. Cukierman S (2006) Et tu, Grotthuss! and other unfinished stories. Biochim Biophys Acta BBA Bioenerg 1757:876–885. https://doi.org/10.1016/j.bbabio.2005.12.001
79. Hodel FH, Luber S (2016) What influences the water oxidation activity of a bioinspired molecular CoII4O4 cubane? An in-depth exploration of catalytic pathways. ACS Catal 6:1505–1517. https://doi.org/10.1021/acscatal.5b02507
80. Mayer JM, Rhile IJ (2004) Thermodynamics and kinetics of proton-coupled electron transfer: stepwise vs. concerted pathways. Biochim Biophys Acta 1655:51–58. https://doi.org/10.1016/j.bbabio.2003.07.002
81. Kozuch S, Martin JML (2012) "Turning over" definitions in catalytic cycles. ACS Catal 2:2787–2794. https://doi.org/10.1021/cs3005264